

弧焊机器人起始焊接位置图像识别与定位

陈希章¹, 陈善本²

(1. 江苏大学 材料科学与工程学院, 江苏 镇江 212013; 2. 上海交通大学 焊接工程研究所, 上海 200030)

摘 要: 起始焊接位置的识别和定位是实现机器人智能化焊接的第一步, 在分析焊缝接头类型的基础上给出了起始焊位的定义. 采用 CCD 摄像机在自然光条件下获得待焊工件图像, 由起始焊位的定义分析了起始焊位识别的方法. 提出一种局部范围内由粗到细的两步精确定位方法. 首先求取焊缝和工件边界交点作为初始值. 第二步以该点为中心建立一个窗口, 在此局部范围内检测角点. 根据设定的判断标准, 可充分利用原图像的丰富信息和边缘提取后的结构化信息. 结果表明, 对规则焊缝, 初始值与实际初始焊位能很好吻合, 而对不规则的焊缝, 初始值偏离实际位置. 文中提出的两步定位方法则能准确的识别和定位具有明显边界的规则和不规则焊缝的初始焊位.

关键词: 起始焊位; 图像识别; 弧焊机器人

中图分类号: TG115.28 **文献标识码:** A **文章编号:** 0253-360X(2009)04-0017-04



陈希章

0 序 言

弧焊机器人起始焊接位置的准确定位是实现高质量焊接的第一步, 工业应用的机器人主要工作在示教再现模式, 在寻找起始焊位时主要靠手工示教, 这除依靠示教经验外还破坏了整个焊接过程, 且当工件位置变化时, 需重新示教. 自主寻找焊缝起始位置方面的研究不多见, 这已引起部分大公司的重视^[1,2], 如日本安川机器人公司、三星电子株式会社洪性濠^[3]采用接触式方法检测出焊接起始点. 但须事先知道起始焊接位置再进行精确定位, 受传感方式限制, 仅适用于 L, V, T 形等明显可探测边界焊缝情况. 焊缝的边缘必须很明显便于接触, 机器人须先移动到焊接起点附近, 在较小区域内而不能大范围的寻找起始焊位, 而且要求较大的工作空间, 应用受限. Kuka 机器人采用激光传感进行焊接起始位置的寻找, 但体积较大, 仅能用来实现导引, 价格昂贵.

机器视觉技术的发展及性能可靠、体积小、价格低的 CCD 传感器的出现使得视觉成为自动控制中常用的传感方法, 丰富的信息量使得它在起始焊位的定位方面的应用成为可能. 采用视觉传感的方法获得焊前工件图像, 用一种由粗到细的起始焊接位

置精确定位方法, 有助于焊接过程的自动化程度和智能化水平, 具有重要意义.

1 起始焊位的定义和分析

对待焊工件, 起始焊接位置可有两个, 即在图像坐标系中坐标值较小侧和较大侧各有一个点, 文中以坐标值较大侧的点作为起始焊位. 对圆形、方形等封闭的焊缝, 没有明确起始焊位的点, 规定以双目视觉系统中左摄像机拍摄到的图像为基准, 将左图像坐标系中点的坐标作为起始焊位, 再求其在右图像中的匹配点. 焊接工程中焊缝主要有对接、角接、搭接和丁字接头形式. 根据实际情况对接接头需加工成各种坡口, 如 V, U, X 形等, 而角焊缝也可有正面、侧面和斜向角焊缝, 丁字接头可看作角焊缝的一种. 图 1 给出了典型的坡口形式, 将这些形式焊缝的起始焊位归结为图 1a, b, c 三类, 称之为 T, L 和 V 形. 三种类型下面的图形是其对应的坡口形式, 图中标识 1 是起始焊接位置一侧的工件边界, 标识 2 和黑色填充部分代表的是焊缝. 其它形式焊缝的起始焊位也可归结到这三类中, 如角接可看作图 1b 类, 若是斜向角焊缝, 则变为虚线所示的 1'; 丁字接头也可类似分析.

起始焊接位置可看作工件边界或坡口 1 与焊缝的交点, 这对应于图像处理中的角点. 因此对于起始焊位的求取, 就有了两种方法, 即求交点和角点.

收稿日期: 2008-01-28

基金项目: 国家自然科学基金资助项目(50575144); 江苏大学高层次人才启动基金资助项目(07JDC085); 江苏大学创新团队基金资助项目(CLXY03)

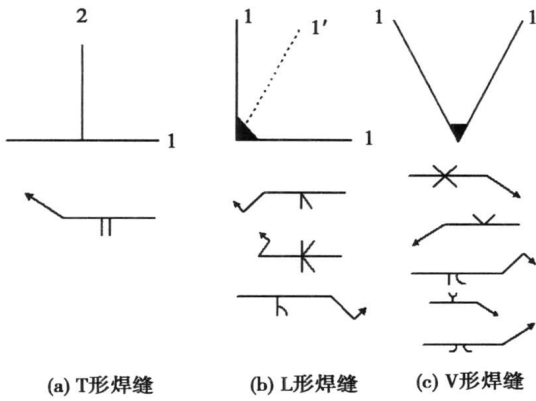


图1 接头形式与起始焊位

Fig. 1 Joint type and initial weld position

采用拟合边缘曲线求取焊缝与工件边界交点的方法可确定起始焊接位置。这对直线类或规则曲线较为准确,但不规则曲线很难用准确的方程来描述曲线,这将导致曲线方程拟合不准确,使得起始焊位的定位不准确。在识别过程中由于各种原因也可能导致焊缝曲线坐标点不连续,采用边缘连接和拟合的方法会因为间断距离和拟合方法问题导致一定误差,从而导致起始焊位最终定位不准确。若直接检测角点,则由于图像中有很多符合角点的特征造成错误的定位。为此,提出在求交点确定起始焊位方法基础上的局部范围内角点检测求定位方法。

2 边缘线相交定位起始焊位

通过焊缝的识别可分离出焊缝的边缘和工件的边界轮廓,具体可参见文献[4]。因此可通过求焊缝与工件边缘的交点来确定起始焊位的坐标。为求此交点,根据数据点集拟合曲线,通常使用最小均方误差准则来找出一定参数形式下的最佳拟合函数。具体选择什么参数形式与问题有关,如通常采用多项式形式特别是二次多项式形式,而对于更为一般的情况也可采用样条函数形式。

设通过图像识别已经得到一个边缘的点集 (x_i, y_i) , $i = 1, 2 \dots n$, 需要找出一个函数 M_{SE} 使其均方误差最小,即

$$M_{SE} = \frac{1}{2} \sum_{i=1}^n [(y_i - f(x_i))]^2 \quad (1)$$

曲线拟合就是确定参数最佳值的过程,这样就可得到曲线方程。文中所有的拟合函数采用一次或二次多项式的形式,将拟合后焊缝曲线和工件边界的方程组成方程组,可求得起始焊位位置在图像坐标系中的坐标,作为起始焊位的初值。

3 局部角点精确定位

如前所分析,起始焊位可通过求取工件边缘线或坡口边缘线与焊缝所形成的角点求取完成。图像处理中,角点的提取和定义有不同的方法,如图像边界上曲率变化明显的点^[5],图像边界上曲率足够高的点^[6],图像边界方向变化不连续的点^[7]等。由这些定义可看出,角点检测的方法也不尽相同,如直接以图像灰度信息检测^[8],用轮廓点计算曲率判定^[9]等。主要角点检测方法可归纳为两类:一是根据图像边缘特征,用轮廓点计算边缘曲率或夹角判定;二是直接利用灰度进行角点检测。前者利用处理后的结构化信息,快速简单,但依赖于前期图像处理的结果,后者直接利用原图信息,但对噪声敏感,精度低。

角点检测时,以上求得交点为初值,以该值为中心确定一个小窗口,仅在该窗口内进行角点提取。设该窗口内边缘线表示为一个有序点集 $S = \{P_i : (x_i, y_i), i = 1, 2 \dots n\}$,这里的有序是指顺时针或逆时针的扫描方向。以点 P 为中心其前后均有 M 个点,是一个联通的区域。前后是指搜索范围内顺时针或逆时针先扫描到的点。如图2a所示,曲线上任意点 P_i 与 P_{i-k}, P_{i+k} 组成一个变化的三角形,则有 $|P_i P_{i+k}| = a$, $|P_i P_{i-k}| = b$, $|P_{i-k} P_{i+k}| = c$, P_{i-k}, P_{i+k} 间的夹角是 $\alpha \in [-\pi, \pi]$,根据三角几何关系得

$$\alpha = \arccos\left(\frac{a^2 + b^2 - c^2}{2ab}\right) \quad (2)$$

如下条件用于判断曲线上的点是否为角点候选点,即

$$\left. \begin{aligned} d_{\min}^2 &\leq a \leq d_{\max}^2 \\ d_{\min}^2 &\leq b \leq d_{\max}^2 \\ \alpha &\leq \alpha_{\max} \end{aligned} \right\} \quad (3)$$

式中: $d_{\min}, d_{\max}, \alpha_{\max}$ 是该约束条件的主要参数, d_{\min} 决定了获得准确角点的最小值, d_{\max} 为最大值,是为了防止三点间隔太远,避免噪声点的影响,如离 P 点很远的点形成锐角三角形,则造成错误的角点检测值。文中参数为 $d_{\min} = 3, d_{\max} = 5, \alpha_{\max} = 150^\circ$ 。

满足该约束条件的点都为候选点,但只有一个正确。确定最终角点方法如图2b所示,设相邻的两个候选点 P 和 P' ,若 $\alpha_P > \alpha_{P'}$,就淘汰 P 而认为 P' 是正确的点。如果有多个点,依此方法可确定唯一的角点。这样经过两个步骤可确定唯一的正确角点。定位过程中直接利用SUSAN角点检测方法^[6]进行

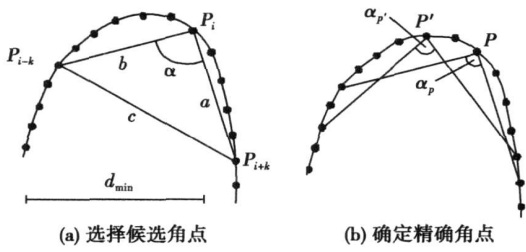


图 2 角点检测过程

Fig. 2 Corner detection

基于灰度的角点检测。

图 3 为起始焊位识别流程示意图。首先识别出

焊缝, 利用分离出的焊缝和工件边缘坐标数据拟合出曲线方程, 对应于图 3 中的 (1); 再利用拟合得到的曲线方程分别求两条平行焊缝与边界的两交点, 以两交点的中点作为起始焊位初值, 对应于图中的 (2); 然后以该初值为基准(图中以 * 号标识), 以其为中心在原图或识别后的图像中确定一个 $M \times N$ 的窗口(参见图中的方框)作为下一步搜索的范围, 对应于流程图中的 (4) 和 (4)'; 第四步是在第二步确定的搜索范围内进行角点提取, 可分别得到焊缝两边与工件边界形成的两个角点, 取两角点的中点作为最终的起始焊位坐标(图中实心句点), 对应于图中的 (5) 和 (5)'。

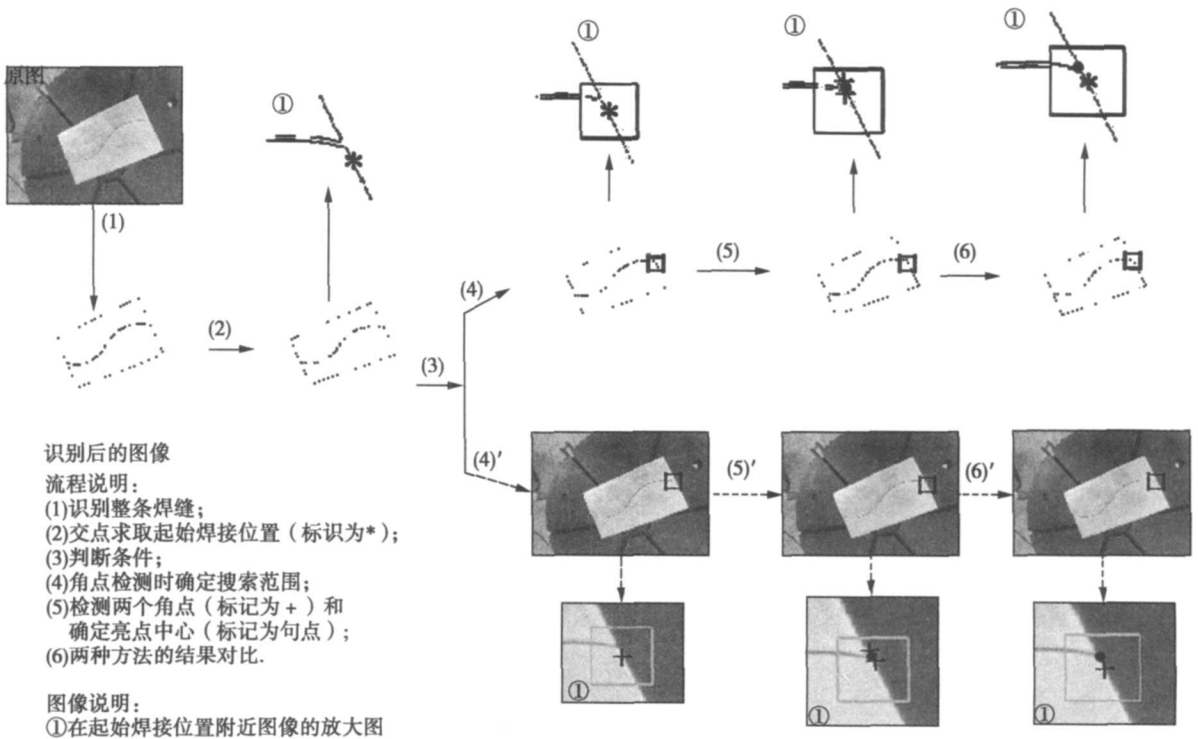


图 3 起始焊接位置识别流程图

Fig. 3 Flowchart for recognition of initial weld position

图 3 在步骤 (3) 处有一分叉, 这是一个用来判断后面的处理采用原始图像还是识别后图像的标准. 该标准的设定是在图像识别的过程中, 即图 3 中步骤 (2), 判断焊缝间断的大小和离工件右边界附近的焊缝是否间断. 若间断过大或起始点附近的数据点没有识别出, 对于复杂不规则焊缝来讲, 通过连接和拟合不能完全反映图像真实信息, 则用原始图像进行边界提取, 过程与利用识别后的图像时相同.

图 3 中的 (6) 是采用求交点方法和采用局部范围内角点搜索方法确定起始焊位结果的比较. 图 4 和图 5 进一步说明该问题, 在两幅图像中 * 标识的是通过求交点得到的起始焊位坐标, 方框是以该点

为中心的窗口. 实心句点标识的是局部范围内角点检测所得到的坐标. 前者是直线焊缝, 由于是直线, 即使不能识别全部的焊缝也能通过拟合得到精确的直线方程, 因此从局部放大图可看出 * 和实心句点完全重合, 即两种方法都可得到准确结果. 图 5 分别用原图和识别后的图像进行了局部角点检测, 该曲线为类似 \sin 函数的不规则曲线, 从放大图看出两线相交求中点的方法偏离了实际的起始焊位, 这是拟合曲线不能完全反映真实焊缝导致的. 从图 5b, d 看出, 采用原图或识别后的图像进行局部角点检测确定起始焊位都可得到与真实位置相吻合的值. 原理上直接利用原图灰度进行角点检测对噪声

敏感,但在较小的范围内,其精度与基于边缘的检测是接近.这说明该图中识别后的图像有足够的信息用于角点检测,这是因为识别过程中焊缝在起始焊位附近没有明显的间断,从而反映并简化了原始图像的信息.在利用识别后的图像和原始图像都能检测出角点的情况下,建议采用基于边缘的方法,因为这种结构化的信息能简化处理过程.

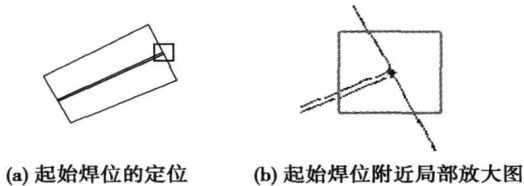


图4 两种起始焊位识别方法一致的情况(直线焊缝)
Fig. 4 Case of identical results by two methods(line seam)

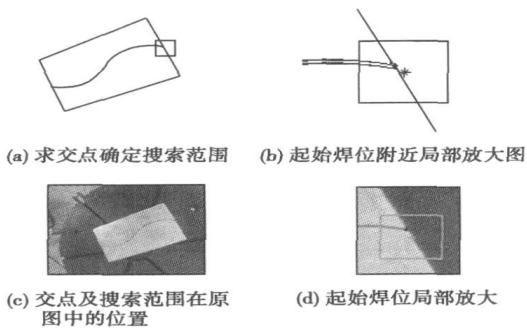


图5 两种起始焊位识别方法不一致的情况
Fig. 5 Case for different results by two method

该方法在局部范围内检测起始焊位,排除了其它因素的干扰,可快速精确的对起始焊位进行定位.定位试验结果也表明采用该方法可准确的对起始焊位进行定位,证明该方法是有效的.

4 结 论

(1) 工件焊缝形式可以分为三类,起始焊接位置的定义可以适用于各种形式的焊缝类型.

(2) 工件的起始焊接位置通过求取交点和角点两种方法来求取.

(3) 提出的由粗到细的两步方法充分利用了图像的丰富信息和识别后简化的结构化信息,可以快速准确的识别和定位规则焊缝和不规则焊缝的起始焊接位置.利用此结果采用机器视觉的方法可以计算出起始焊位的三维信息,实现起始焊位的导引.

参考文献:

- [1] 朱振友. 焊接机器人初始焊位视觉识别与导引研究[D]. 上海: 上海交通大学, 2004.
- [2] Chen X Z, Chen S B, Lin T, *et al.* Practical method to locate the initial weld position using visual technology[J]. *International Journal of Advanced Manufacturing Technology*, 2006, 130(7-8): 663-668.
- [3] 洪性漆. 机器人初始焊接位置检测方法: 中国, 98105416. 1[P]. 1998-03-03.
- [4] Chen X Z, Chen S B, Lin T. Recognition of macroscopic seam for complex robotic welding environment[J]. *Lecture Notes in Control and Information Sciences*, 2007, 362: 171-178.
- [5] Zuniga O A, Haralick R M. Corner detection using the facet model [C] // *Proc Conf Computer Vision and Pattern Recognition*. Washington D C, 1983: 30-37.
- [6] Smith S M, Brady J M. SUSAN-a new approach to low level image processing[J]. *International Journal of Computer Vision*, 1997, 23(1): 45-78.
- [7] Sheu H T, Hu W C. A rotationally invariant two phase scheme for corner detection[J]. *Pattern Cognion*, 1996, 29(5): 819-828.
- [8] Freeman H, Davis L S. A corner finding algorithm for chain code curves [J]. *IEEE Trans on Computers*, 1977, 26(3): 297-303.

作者简介: 陈希章,男,1976年出生,博士,讲师.主要研究方向为机器人焊接智能化、新材料焊接和机器视觉等.发表论文20篇.

Email: kemel.chen@gmail.com

MAIN TOPICS, ABSTRACTS & KEY WORDS

Study on microstructure of the coatings sprayed in low pressure condition and its post treatment technology

LI Deyuan, SONG Dan, ZHANG Zhongli, ZHAO Lingyan (School of Materials Science and Engineering, Shenyang University of Technology, Shenyang 110178, China). p1-4

Abstract: In order to make clear the effect of the spraying technology on the coatings microstructure formation in the low pressure spraying, the wires of 4Cr13, Al and Ti were adopted to prepare the spraying coatings in air and low pressure condition, respectively. The microstructure, the amount of the compounds and their distribution pattern in both coatings were compared by the micro-analysis and micro-area chemical analysis. Static press test was used to investigate the closing possibility of the porosities. After the press test, the coatings was heated to certain temperature to analyze the effect of the recrystallization heat treatment on the coatings microstructure. As a result, the amount of the oxide in 4Cr13 and Al coatings has been reduced obviously in the low pressure condition, and metallurgy combination between the splat particles can be formed by pressing and heating. However the low pressure condition can not provide sufficient protection for the Ti coatings, the following recrystallization heat treatment can not get metallurgy combination between the particles.

Key words: arc spraying; coatings; spraying particle; oxide; recrystallization

Full digital control of *I/I* mode pulsed MIG welding based on triple closed loop control

SHA Deshang, Liao Xiaozhong (School of Automation, Beijing Institute of Technology, Beijing 100081, China). p5-7, 12

Abstract: This paper presents a full digital control strategy for pulsed MIG/MAG welding based on digital signal processor (DSP) control. One droplet per one pulse (ODPP) is maintained with the proposed control strategy which is characterized by *I/I* mode with adaptive voltage compensation (AVC). Welding database with different materials and diameters is established according to wire feed speed. Arc length is detected during each pulse period and the melting rate is changed. Moreover, real time compensation for the volt drop across the wire stickout is made to ensure the arc length constant while stickout changing. Operation principles are analyzed and control block diagram composed of triple closed loop is also presented. Experimental results show that the proposed method is feasible and universal. Constant arc length is realized when wire stickout changes. The welding process is stable and the welding bead is also good with the proposed method.

Key words: pulsed MIG welding; full digital control; arc length

Stereovision-based detection of 3-D weld seam using epipolar line constraint and laser stripe indication

LI Hexi^{1,2}, WANG

Guotong¹, SHI Yonghua¹, ZHANG Weimin¹ (1. College of Mechanical and Automotive Engineering, South China University of Technology, Guangzhou 510640, China; 2. College of Information Engineering, Wuyi University, Jiangmen 529020, Guangdong, China). p8-12

Abstract: An epipolar line constraint equation is established for a binocular stereovision system mounted at the end-effector of welding robot. The stereovision correspondence technique based on the combination of epipolar line constraint with laser stripe indication is applied to detect the position of a three-dimensional (3-D) saddle-shaped weld seam which is produced by the intersection of two circular pipes. The experimental results show that the smooth segments of laser stripe in the weld seam image can be obtained using thinning and deburring arithmetics, and the stereovision correspondences between pairs of points at the left and the right images can be dependably realized by detecting both the singular points of laser stripe curvature and the intersecting points of laser stripe with epipolar lines, thus the detection accuracy to the 3-D weld seam and its adjacent area can be improved. The geometrical shape of the 3-D weld seam is reconstructed from the 3-D data acquired by stereovision-based detection with less errors compared with its actual dimension, therefore the proposed method can satisfy the detection requirement of 3-D weld seam in automatic robot welding system.

Key words: stereovision; epipolar line constraint; laser stripe indication; correspondence; weld seam detection

Plasma component calculation in underwater wet welding

LI Zhigang, ZHANG Hua, JIA Jianping (Institute of Mechatronics Engineering, Nanchang University, Nanchang 330031, China). p13-16

Abstract: The electric arc is formed in the ionized gas bubble in the underwater wet welding. Combined with the previous bubbles components determination, the main ionization and dissociation process in the bubble are analyzed. The calculation based on the potapov model was done for the underwater arc components at different water pressures and temperatures under the local thermodynamics equilibrium state. Its main theoretical bases are the Dalton law of partial pressure, the law of mass action, the electric charge quasi-neutrality condition and the chemistry measurement equilibrium condition. The results show that with the pressure increasing from 0.1013 MPa to 1.013 MPa and then to 10.13 MPa, the density of H, H⁺, O, C, O⁺, C⁺ is increased, but the average ionization degree is not influenced by the water pressure.

Key words: underwater wet welding; electric arc; components calculation

Recognition and positioning of start welding position for arc welding robot

CHEN Xizhang¹, CHEN Shanben² (1. School of Material Science and Engineering, Jiangsu University, Zhenjiang

212013. Jiangsu, China; 2. Institute of Welding Engineering, Shanghai Jiao Tong University, Shanghai 200030, China). p17–20

Abstract The recognition and positioning of start welding position (SWP) is the first step to realize intelligent robot welding. The definition of SWP is given based on the analysis of seam type. The macro-scopical images of workpieces to be welded are snapped by CCD camera in a relatively large range without additional light. The recognizing methods of SWP are analyzed according to its definition. A two-step method that from coarse to fine is proposed to recognize the SWP accurately. The first step is to solve the curve functions of seam and workpieces boundaries by fitting, and their intersection points are regarded as the initial value of SWP. The second step is to establish a small window that takes the initial values as the centre. And the SWP becomes exact by the corner detection in the window. Both the abundant information of original images and the structured information of recognized images are used according to the given judge rules, which take full advantage of the image information and improve the recognized precision. The detected results show that the actual position of SWP and recognized initial value by the first step are identical for the normal seam, but the recognized result by the first step is different from the actual position for the un-normal curve seam. The exact results can be obtained by the presented two-step method for both normal and un-normal curve seams.

Key words: start welding position; image recognition; arc welding robot

Cracking control technology of TiC/Ni coatings prepared by in-situ fabrication through laser cladding HE Qingkun, WANG Yong, ZHAO Weimin, CHENG Yiyuan (Material Department, College of Mechanical and Electronic Engineering, China Petroleum University, Dongying 257061, Shandong, China). p21–24

Abstract There are many cracks in TiC/Ni coatings prepared by in-situ fabrication through laser cladding. The reasons for crack initiation in the coatings were analyzed from the microstructure, the phase composition, the residual stress, the macro morphology and the fracture observation. Corresponding cracking control measures were also proposed. The investigation indicated that the cracks of the TiC/Ni coatings are mainly brittle cold cracks caused by hard brittle phases and internal residual stress. The replacement reaction ($M_{23}C_6 + Ti \rightarrow M + TiC$) occurs by increasing the content of Ti powder. Therefore, cracks of the coatings can be reduced or eliminated. Moreover, intriguing microstructures of the coatings are obtained with enhanced plasticity and toughness and reduced residual stress by nickel powder addition or by optimizing processing parameters, thus the cracking susceptibility can be decreased.

Key words: in-situ fabrication; laser cladding; cracking control; replacement reaction

Welding distortion prediction and control of thin plate welded structures of the truck side-walls LI Yana, ZHAO Wenzhong, LU Bihong, NIE Chungu (School of Traffic Transportation, Dalian Jiaotong University, Dalian 116028, Liaoning, China). p25–28

Abstract: During the process of the truck side-walls weld-

ing, buckling deformation is caused by the shrinkage force in the weld seams. It is difficult to predict and control the distortion. The buckling deformation which not only reduces the strength but also affects the smoothness and the beauty of thin-plate. The welding distortion of the truck side-wall was studied using inherent strain as an equivalent load. The results show that the predicted results is consistent with the measured data. Based on the simulation model, the different factors involved in the design and welding affecting the distortion were investigated using the orthogonal design. The optimal design is presented, which provides reliable theoretical references for thin-plate welding deformation controlling of the truck side-walls.

Key words: thin-plate welded structure; welding distortion; inherent strain; orthogonal design

Numerical simulation of RSW temperature field during aluminum alloys LB-RSW LI Yongqiang¹, Zhao He², Zhao Xihua¹, Jiang Wenhua³, Zhang Weihua¹ (1. School of Materials Science and Engineering, Jilin University, Changchun 130022, China; 2. State Key Laboratory of Advanced Welding Production Technology, Harbin Institute of Technology, Harbin 150001, China; 3. R & D center, FAW, Changchun 130011, China). p29–32

Abstract The thermo-structural and thermo-electrical circular order analyses of resistance seam welding (RSW) process in laser beam-resistance seam welding (LB-RSW) were carried out by means of ANSYS, and the influences of RSW current, welding speed and the space between two RSW wheels on temperature field in RSW were studied. The results indicate the surface temperature of aluminum alloy plates and the temperature gradients both in front and back of wheels increase consequently with RSW current increasing. Meanwhile, the maximum temperature value presents direct ratio relationship with the square of current approximately. The surface temperature of aluminum alloy plates reduces with the increase of welding speed. However, the rate of temperature change appears a converse tendency when the welding speed increases. Besides, the maximum surface temperature of aluminum alloys plates decreases with the decrease of the space between two RSW wheels. Furthermore, the temperature gradient behind the RSW wheels also decreases when the space between the two wheels decrease. The simulation results match well with the thermography acquired by infrared thermography technology, which makes it feasible to predict the optimal relative position between laser beam and resistance heat source and to investigate the mechanism of LB-RSW.

Key words: resistance seam welding; laser welding; temperature field; numerical simulation

Temperature field simulation of electron beam rapid prototyping

CHEN Yunxia, ZHU Miaofeng, LU Fenggui, YAO Shun (Welding Engineering Institute, Shanghai Jiaotong University, Shanghai 200240, China). p33–37

Abstract The temperature field of electron-beam rapid prototyping is simulated by ANSYS. In this study, heat distribution is expressed as Gaussian equation. The heat loss just includes heat radiation as the process is carried out in the vacuum chamber. Tem-